Journal Name

ARTICLE

Pressure-induced switching properties of the iron (III) spin transition complex [Fe^{III}(3-OMeSalEen)$_2$]PF$_6$

J. Laisney, [‡a] H. Shepherd, [b] L. Rechignat, [c] G. Molnár, [c] E. Rivière [a] and M.-L. Boillot [*a]

We investigated the effect of an externally applied pressure on the iron (III) Schiff-base compound [Fe(3-OMeSalEen)$_2$]PF$_6$ (H-3-OMeSalEen, condensation product of 3-methoxy-substituted salicylaldehyde and N-ethylethylenediamine), which at ambient pressure displays a thermal spin transition with a 3 K wide hysteresis loop centered at 164 K. Raman spectrometry revealed the occurrence of a complete spin-state switching process for a pressure of P$_{1/2}$ = 8-9 kbar at room temperature. The evolution of lattice parameters as a function of pressure was followed by X-ray diffraction measurements on single crystals, highlighting the important microscopic aspects at the origin of the pressure-induced transition, i.e. an anisotropic response and a high compressibility of the HS molecular lattice. Variable temperature magnetic susceptibility measurements at different applied pressures revealed the smoothening of the spin transition curves and a linear increase of the transition temperatures by ca. 16.4 (1.0) K/kbar – in good agreeement with the Clausius-Clapeyron law. The non-negligible influence of the pressure transmitting oils on the intrinsic transition properties was also evidenced and attributed to mechanical interactions between the particles and the solidified matrix.

1. Introduction

Among the miniaturizable functional materials that are currently targeted for applications, switchable molecular materials that undergo cooperative and hysteretic phase transformations[1,2] based on the spin-crossover phenomenon, represent a class with decisive advantages[3] (for information storage, sensing or actuators). The transition between the low-spin (LS) and the high-spin (HS) state of the metal ion proceeds via an electron-phonon coupling and thus, is accompanied by an increase of the coordination volume[4] (V$_{HS}$ ~ 12 Å^3 and V$_{LS}$ ~ 9 Å^3 in case of Fe(II) compounds) that influences all the physical characteristics (optical, magnetic, vibrational, structural, electrical, mechanical and thermophysical properties). The study of how such solids react to mechanical stress is thus of fundamental importance for studying the

stability of the solid phase and the elastic properties that govern the cooperativity. It is also vital for analyzing of volume-dependent properties as well as for triggering the spin-state switching if such a process is possible.

In the literature, this topic has been investigated with polymeric coordination networks and molecular compounds, selected among the cooperative and bistable materials.[5-9] The application of a hydrostatic pressure to SCO-active materials usually shifts the thermal SCO curve to higher temperature and reduces the thermal hysteresis. It also induces a HS to LS switching at a given temperature and may trigger structural changes (including phase transition) that lead to more complex behavior.[10] The degree of cooperativity in a transition resulting from elastic forces between individual SCO sites has been rationalized with the image-pressure model, based on continuum mechanics considerations,[11] which was successfully applied to metal-dilution experiments,[12] and later on, with different microscopic models.[13] These studies were conducted chiefly with Fe(II) compounds, which are typically the most cooperative SCO materials, owing to their larger volume change on SCO.[14-17] Such studies on Fe(III) compounds are less frequent,[18,19] especially those which exhibit a first-order spin transition.[20]

In this context, the possibility of generating cooperative elastic interactions that drive the self-amplification of the spin-state switching in the out-of-equilibrium state of a SCO solid was recently demonstrated by using ultrafast laser excitation.[21] This study was achieved with a first-order spin transition Fe(III)

compound, [Fe(3-OMeSalEen)$_2$]PF$_6$ that some of us prepared in form of nano-, micro- and macroscopic single-crystals.[22]
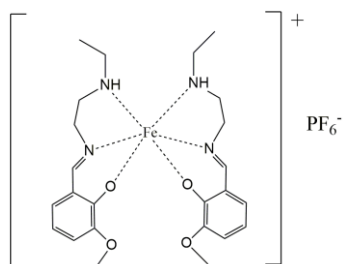
Scheme 1 Molecular structure of [Fe(3-OMeSalEen)$_2$]PF$_6$

In the present work, we focus on the latter Fe(III) compound whose behavior under mechanical stress has not been investigated. The objectives of this study are to establish the structure-property relationship under pressure and to determine the conditions for switching the spin states with pressure at ambient temperature. The [Fe(3-OMeSalEen)$_2$]PF$_6$ Schiff-base compound[23] (scheme 1) undergoes a cooperative S = 1/2 $\leftrightarrow$ S = 5/2 spin transition with a 3 K wide thermal hysteresis centered at 164 K.[24] The process is coupled to an isostructural phase transition of the lattice consisting in pairs of complexes packed in a 3D network through intermolecular (π-π and Van der waals) interactions. Our work was conducted with crystals by using complementary structural (single-crystal X-ray diffraction), vibrational (Raman spectrometry) and magnetic (susceptometry) techniques for studying the macro- and microscopic features of the multiscale processes under pressure. For the specific needs of the different experiments, we employed three different pressure-transmitting media, which have been used then also to demonstrate specific matrix effects.

2. Results

The change in the thermal SCO under applied pressure was characterized by magnetic measurements. Then the pressure-induced HS to LS state switching taking place at room temperature was probed with Raman spectroscopic and X-ray diffraction measurements.

2.1 Pressure effect on the thermal spin-transition

The diamagnetic, clamp-type pressure cell, made of hardened beryllium bronze,[25] allows a hydrostatic pressure to be applied to an ensemble of small single-crystals dispersed in a pressure transmitting mineral oil (Alcatel 100). Prior to collecting the magnetic data under an applied pressure, we have characterized the χ_MT $vs.$ T curve (χ_M = molar magnetic susceptibility corrected for diamagnetic contributions) of the sample both in the presence and absence of the oil. Figure 1 shows the first-order spin transition of the pure solid with the expected characteristics (here, T$\downarrow$ = 162 K, T$\uparrow$ = 164 K) and limit values (χ_MT = 0.40 and 4.10 cm^3 mol^{-1} K at 100 K (S = 1/2) and 200 K (S = 5/2), respectively) at a scanning rate = 0.5 K min^{-1}.

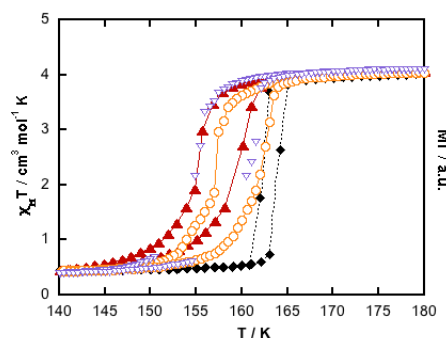Fig. 1 Temperature dependence of χ_MT of [Fe(3-OMeSalEen)$_2$]PF$_6$ in form of crystals (◆), dispersed in Alcatel 100 (▲) and Fluorinert FC77 (○) oils, recorded between 180 and 140 K with a scanning rate of 0.5 Kmin^{-1}. The MxT $vs.$ T data (see Fig. S7) obtained with the dispersion in Daphne 7373 oil (▽) were also scaled in order to get a comparison between the spin-transition temperatures.

When the powder is dispersed in the mineral oil, the completeness of the transition is preserved in both directions, but the transition curve is shifted to lower temperatures (by 6 K) and becomes less abrupt. On the other hand, the hysteresis width increases by 2 K (T$\downarrow$ = 155 K, T$\uparrow$ = 159 K and T$_{1/2}$ = T$\downarrow$-T$\uparrow$ = 157 K). We can thus conclude that the medium used for ensuring a hydrostatic pressure all over the sample influences the magnetic behavior of the compound. This matrix effect is similar to that previously reported for the compound Fe(phen)$_2$(NCS)$_2$ (phen: 1,10-phenanthroline).[26] This effect has been also confirmed with the other pressure-transmitting media used in this study (Figure 1).

The magnetization (M) vs. T curve of the in-oil dispersion placed within the pressure cell was recorded at a rate of 0.5 Kmin^{-1}, for pressure values varying between 0 and 6.5 kbar. Each thermal cycle was reproduced twice to ensure data reproducibility. Figure 2a shows the superposition of the magnetization curves. The plot at P = 1 bar is consistent with that measured out-of-the cell in the presence of oil despite some anomalies in the region where the magnetization signal vanishes (i.e. where the measurement error diverges). When the pressure increases, the spin transition curve shifts towards higher temperatures (see Table S1 in SI), becomes more gradual and the width of the apparent hysteresis decreases. At a pressure of 6.5 kbar, that is the highest value studied here, the transition occurs very close to ambient temperature. The 6.5 kbar transition curve occurs with apparent steps, which are also discernible in the 4.8 kbar curve. This observation may suggest a two-step process. However, possible artefacts due to the signal vanishing around M = 0 and/or other due to the solidification of the oil cannot be ruled out (see below) and thus further experimental investigation is required to clarify this point. After the complete releasing of pressure, the magnetization curve was again recorded and the reversibility of the pressure-induced modifications was confirmed (Figure S1 in SI).
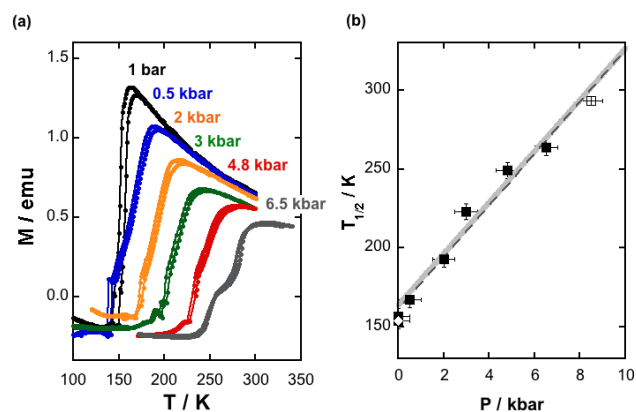
Fig. 2 (a) Magnetization as a function of temperature measured for various applied pressure values (P = 0-6.5 kbar) for the compound [Fe^{III}(3-OMeSalEen)$_2$]PF$_6$ in form of a dispersion of single-crystals in the Alcatel oil (scanning rate: 0.5 K.min^{-1}). (b) Evolution of the transition temperature $T_{1/2}$ as a function of the pressure P determined by magnetic (■), X-ray diffraction (+) and Raman spectrometry (□) measurements on single crystals of [Fe^{III}(3-OMeSalEen)$_2$]PF$_6$. In red is shown the point measured after decompression (■). The dotted and grey lines are the fitted and calculated Clapeyron slopes, respectively.

Fig. 3 (a) Selected Raman spectra recorded at room temperature between 1 bar and 12 kbar. (b) The value of the I_{566}/I_{630} relative Raman intensity plotted as a function of pressure (●) and after decompression (♦, P = 1 bar). Inset: Images showing the spin crossover of crystals taking place between P = 1 bar (HS, after decompression) and P > 9 kbar (LS).

The transition temperature ($T_{1/2}$) that corresponds to a 50% completeness of the spin-crossover was plotted as a function of the applied pressure in Figure 2b revealing a monotonous upshift of $T_{1/2}$ by ca. 16.4 ± 1.0 K/kbar denoting the stabilization of the LS phase. This monotonous variation of the SCO curve under pressure suggests that no other process (e.g. crystallographic phase change) occurs in this pressure range. Then, an extrapolation of these data to room temperature indicates that an applied pressure of ~ 8 - 8.5 kbar would be necessary in order to observe the pressure-induced spin crossover. These high-pressure experiments at ambient temperature were conducted using Raman and XRD techniques in conjunction with a diamond anvil cell (DAC).

2.2 Pressure-induced spin-crossover at room temperature

2.2.1 Raman measurements

Raman spectrometry is a powerful technique that enables the analysis of both vibrational modes belonging to the molecular skeleton and the crystal lattice, and their variation in response to a stimulus, pressure in this case. To assess reference spectra for the HS and LS states, we recorded first high quality variable temperature spectra at atmospheric pressure with the single-crystal out of the pressure cell (see Figure S2 in SI). The decrease of the temperature from 262 to 113 K produces important changes in frequencies and intensities typical of the SCO process (Table S2 in SI) as previously reported in case of nanocrystals dispersed in PEG.[22] We consider the peak at 566 cm^{-1} assigned to the HS molecules and the peak convolution around ca. 630 cm^{-1} found for the HS and LS molecules. The plot of the relative intensity variation I_{566}/I_{630} *vs.* temperature was found to satisfactorily reproduce the magnetic behavior (Figure S3) and thus, this ratio was used in the following analysis.

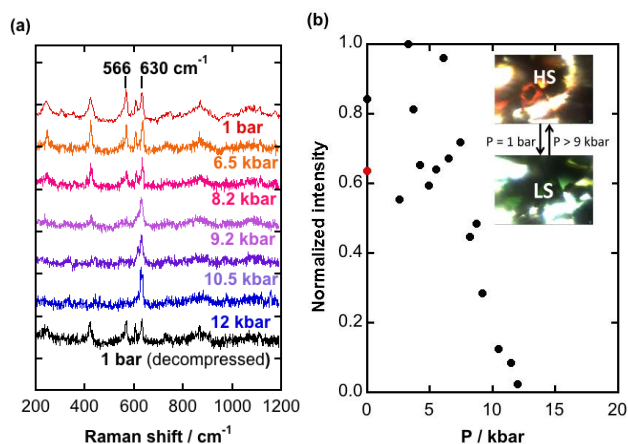Figure 3a (see also Figure S4) shows the room temperature Raman spectra recorded between P = 1 bar and 12 kbar.

For that, a single-crystal was embedded in the Daphne 7373 oil, which also modifies the transition temperature at ambient pressure (see Figure 1). As expected, the HS markers especially observed in the 200-1000 cm^{-1} range (peaks at 420 ± 4 cm^{-1}, 566 ± 4 cm^{-1} and 606 ± 4 cm^{-1}) prevail in the ambient conditions (P = 1 bar), but they progressively disappear with the application of pressure in comparison to the peak centered at 630 ± 4 cm^{-1} found in both forms (see Table S2 in SI). Figure 3b shows the relative normalized intensity I_{566}/I_{630} as a function of the applied pressure. In the low-pressure range (P < 8 kbar), some fluctuations of the relative signal occur, which result from the relatively weak spectral intensity (i.e. low signal-to-noise ratio). Between 8 - 9 kbar, a very clear jump of I_{566}/I_{630} characterizes the HS to LS state switching and finally, between 10 and 12 kbar, the LS state becomes more stable. The spin crossover was also visually observed during the Raman experiment from the drastic color change of the crystals (see inset in Figure 3b) under compression above 9 kbar (dark green, LS state) and after the pressure releasing (orange, HS state). From the Raman data, a virtually complete and reversible pressure-induced spin transition can be inferred at room temperature. The pressure value at which the SCO occurs at ambient temperature ($P_{1/2}$ ~ 8-9 kbar) fits well with the linear correlation determined from the magnetic measurements (Figure 2) despite the different pressure-transmitting medium used.

2.2.2 Single crystal X-ray diffraction measurements

The low-symmetry of the sample and the angular restrictions of the DAC result in low data completeness during high-pressure single-crystal diffraction studies, precluding structure refinement. As such, single crystal diffraction was used to analyze the triclinic unit-cell parameters as a function of pressure up to 15 kbar at ambient temperature. For the XRD experiment, we used the Fluorinert FC77 as the pressure-transmitting medium.
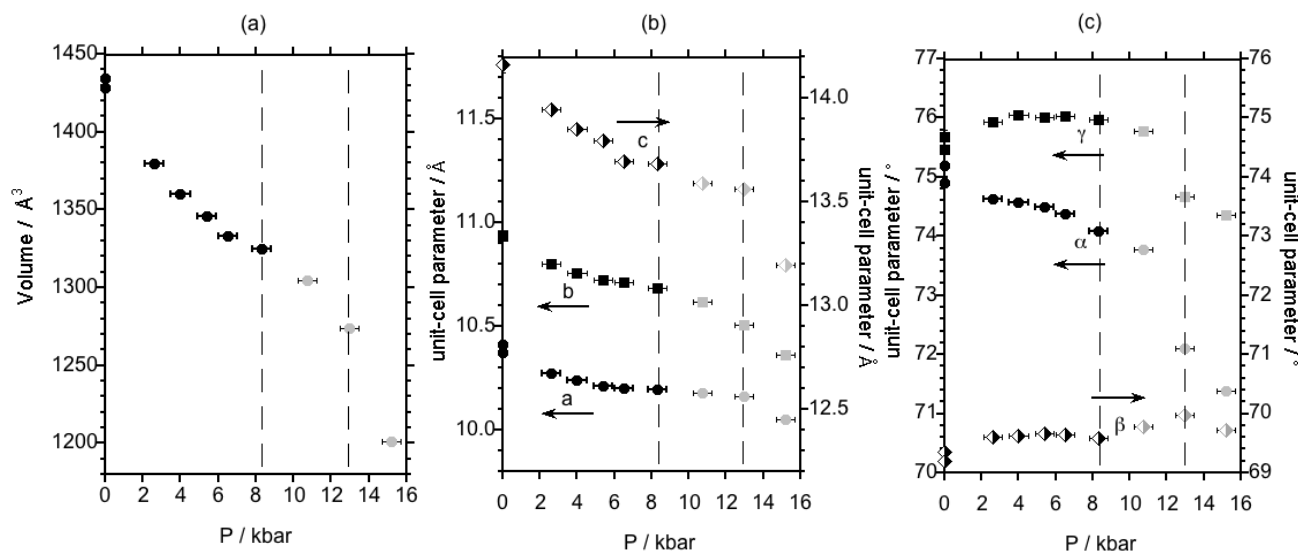
Journal Name

ARTICLE

Fig. 4 Evolution of the trigonal unit-cell parameters of [Fe^{III}(3-OMeSalEen)$_2$]PF$_6$ under the effect of pressure: the volume (a), the *a*, *b* and *c* axes (b) and the *α*, *β* and *γ* angles (c). In grey are shown the data recorded above the transition pressure (P$_{1/2}$) at room temperature. Errors on ordinate values are within the spot sizes. The plots of the temperature dependence of the unit-cell parameters are shown for comparison in Fig. S5 (SI).[24]

The SCO curve of the ensemble of small single-crystals embedded in this oil (Figure 1) shows a 5 K wide hysteresis centered at 160 K, which is similar to those recorded with the Alcatel 100 and Daphne 7373 oil. The pressure dependence of the absolute unit-cell parameters is shown in Figure 4 (See also Figure S5 in the SI for the plots of relative parameters vs. P at T$_{amb}$ as well as vs. T at P$_{atm}$). By increasing the pressure, the unit-cell volume considerably compresses by ca. 16 % at 15 kbar. The measurements performed after decompression (P = 1 bar) give values found within the error of the initial ambient values. This confirms the reversibility of the process, although the quality of the crystal deteriorates upon the measurement. The non-monotonous volume vs. P plot shows quasi-linear regions separated by slopes breaking, for instance between 8 kbar, where the contraction relative to the volume at atmospheric pressure reaches 8 %, and 10 kbar. The change of volume taking place in this pressure interval, (ΔV$_{SCO}$)$_P$ = 19.8 / Z Å^3 (with Z = 2) reveals a piezo-induced SCO, as indicated by the Raman measurements and the similar ΔV value ((ΔV$_{SCO}$)T = 21 / Z Å^3, Figure S5) characterizing the thermal SCO.[24] A second discontinuity observed beyond 12 kbar (also in the *β* vs. P plot), may be indicative of a structural phase transition but this point cannot be guaranteed in absence of a full structure refinement. Slightly anisotropic variations characterize the pressure dependence of *a*, *b* and *c* parameters (between 0 and 15 kbar, Δc/c = -6.8%; Δb/b = -5.3%, Δa/a = -3.5%). Concerning the variations of *α*, *β* and *γ* unit-cell angles, one observes between 8.3 and 12.9 kbar a relative increase of *β* and a

decrease of *α* and *γ* that were expected from the comparison with the thermal SCO. Applied to the *a* and *c* unit-cell axes, this analysis is not so straightforward (trend only reproduced with *b* axis) presumably because of the high compressibility of the sample. Moreover the gap between the *β* values measured at 0 and 2.6 kbar that widens after the final decompression of the solid may be tentatively assigned to the single-crystal quality that was damaged by the mechanical stress, as indicated by the increasing of the error bars upon the experiment. Finally it can be noted that under pressure the single-crystal more easily contracts along the *c* axis, which corresponds to the thickness of the thin platelets (Figure S6 in SI).

3. Discussion

A combination of techniques were used to probe the effect of hydrostatic pressure on the first-order spin-transition of an Fe(III) compound in the form of single-crystals. By increasing the pressure, we observed the progressive stabilization of the LS phase, then the room temperature spin-state switching as well as the related changes in structural and vibrational characteristics of the solid.

3.1 Reversibility of the pressure effects

After the decompression stage, we found magnetic, vibrational and structural responses that are comparable to those of the initial crystalline material and that, for distinct ranges of

applied pressure (0-6.5, 0-12 or 0-15 kbar) and different pressure-transmitting media (Alcatel 100, Daphne 7373 and Fluorinert FC77). Nevertheless an apparent decrease of crystallinity may well be associated with some drifts in different metrics (magnetism, $T_{1/2, \text{decompressed}}$ = 154 K; $T_{1/2, \text{initial}}$ = 157 K, Raman spectra, $I_{566}/I_{630,\text{decompressed}}$ = 0.64 and $I_{566}/I_{630,\text{initial}}$ = 0.84, x-ray data $V_{\text{decompressed}}$ = 1028 Å^3, V_{initial} = 1034 Å^3) – even if these drifts are close to experimental errors associated with the different techniques.

This phenomenon has to be considered in relation with the effects of mechanochemical treatments, which notably perturb the spin-crossover behavior as it was previously shown with the compound under study.[23,27] The grinding of [Fe^{III}(3-OMeSalEen)$_2$]PF$_6$ results among other things in a low temperature shift of the magnetic curve as observed here, the incompleteness (significant fraction of HS residue) and the smoothening of the process. These changes were accounted for by the increase in the total surface area of grains and lattice defects.[23] From our X-ray diffraction measurements, it appears that the transformation induced by a pressure of 15 kbar damages the crystal. The variation of the unit-cell parameters after decompression rather suggests a weak LS residue either associated with the solid imperfections or a hypothetical irreversible phase transition occurring at high pressure. Concerning the reversibility of the magnetic response after decompression, the slight apparent changes may be also related with mechanical effects arising from the particle-matrix interactions (see section 3.4).

3.2 Analysis of the material compressibility at room temperature

A 16 % change of the unit-cell volume of [Fe^{III}(3-OMeSalEen)$_2$]PF$_6$ observed when applying a pressure of 15 kbar at room temperature was demonstrated above. The pressure dependence of the unit-cell parameters may be exploited to gain further insights into the response to stress and the compressibility. Some limitations being observed at high-pressure (small number of LS data, quality of hydrostaticity), we could determine the bulk modulus B_0 only in the HS phase (from a Birch-Murnaghan equation of state).[28] The bulk modulus B_0 = 43 (7) kbar is displayed in the Table 1 with the still scarce data collected for spin-crossover compounds and related Prussian blue analogues. The value that roughly compares with that of the ionic complex[29] [Fe(ptz)$_6$](BF$_4$)$_2$ (ptz = 1-propyl-tetrazol) characterizes a highly compressible and soft HS material. Relatively higher values of B_0 (80-110 kbar) are found in the case of HS Fe(III) (or Fe(II)) molecular compounds without any counter-ion or flexible alkyl chain (like ethyl or propyl) on the ligand skeleton. The fact that the compressibility does not necessarily decrease by insertion of a solvent molecule in the lattice is consistent with the prevailing importance of the molecular packing. As expected, the LS materials are found to be relatively stiffer (B_0 = 110-120 kbar), but again some slight variations appear between ionic and neutral complexes. Regarding the coordination polymers, we observe the strong enhancement of stiffness in the HS and

LS networks that result from the chemical interconnection of metallic centers.

Also shown by the variation of the unit-cell parameters of [Fe^{III}(3-OMeSalEen)$_2$]PF$_6$, the compression of the unit-cell takes place in an anisotropic manner. The system being triclinic, the strongest compressibility value in the HS phase is found along a direction having a relatively large projection on the c and b axes. That was not unexpected since the packing consists in a 2D arrangement of dimers of SCO cations with strong intermolecular interactions (Fig. S5) and these planes are separated along the c axis by anionic planes also incorporating the flexible ethyl groups. We also note that along the a and b axes, the packing of the HS phase is partly locked by the face-to-face and CH-to-face π contacts within the dimers of cations which should also influence the compressibility.

Table 1 Bulk modulus data (in kbar) for spin-crossover materials and analogues under pressure (kbar).

Compound	Bulk Modulus; method	Metal center	P	Ref.
[Fe(ptz)$_6$](BF$_4$)$_2$	48.1±0.6; ζ	HS Fe^{II}	-	29
Fe(phen)$_2$(NCS)$_2$	93.5; φ	HS Fe^{II}	10^{-3}	30
	122.0; φ	LS Fe^{II}	10	
Fe(btz)$_2$(NCS)$_2$	82.6; φ	HS Fe^{II}	10^{-3}	30
	121.9; φ	LS Fe^{II}	10	
Fe(dpp)$_2$(NCS)$_2$.py	106.4	HS Fe^{II}	≤4.8	10
[Fe(3-MeOSalEen)$_2$]PF$_6$	43 ± 7; φ,ξ	HS Fe^{III}	10^{-3}	This work
[Fe(TPA)(TCC)]SbF$_6$	108 ± 10; φ,ξ	LS Fe^{III}	≥4	19
Fe(HB(trz)$_3$)$_2$	115 ± 20	LS Fe^{II}	10^{-3}	31
[{Fe(bpp)(NCS)$_2$}(4,4'-bpy)].2MeOH	62 ± 4	HS-HS Fe^{II}	10^{-3}	32
Ni/[Fe(CN)$_6$] *Size 3 nm*	303 ± 38	85% LS-Fe^{II}, 15% LS-Fe^{III}	10^{-3}	33
Ni/[Fe(CN)$_6$]▯ *Size 115 nm*	245 ± 32	10% LS-Fe^{II}, 90% LS-Fe^{III}	10^{-3}	33
Co/[Fe(CN)$_6$]	430 ± 20	LS-Co^{III}, LS-Fe^{II}	>20	34
RbMn[Fe(CN)$_6$]	230 ± 20; ψ	HS-Mn^{II}, LS-Fe^{III}		35
	300 ± 30; ψ	HS-Mn^{III}, LS-Fe^{II}		

φ, ▯▯▯▯ compressibility measurements; ζ, from elastic constants determined by Brilloin spectroscopy; ξ, from the Birch-Murnaghan equation of states in reference 28; ψ, Bulk modulus extracted from reflectivity measurements of the low- and high temperature phases (150 and 850 bar).

It is interesting to notice that the two SCO compounds [Fe^{III}(3-OMeSalEen)$_2$]PF$_6$ and Fe^{II}(phen)$_2$(NCS)$_2$[30] exhibit a closely resembling cooperative first-order spin transition associated to a 2-3 K wide thermal hysteresis centered at ca. 164 and 178 K, respectively. It can be noted here that these rather similar SCO features (cooperativity and transition temperature) derive

from distinctive characteristics of stiffness, anisotropy and molecular volume change upon the SCO.

3.3 Spin-crossover process triggered by pressure at room temperature

Above 8.4 kbar, the decrease of the unit-cell volume induces the SCO of the metal ion. The structural evidence, i.e. the discontinuous variation of parameters, the value of $(\Delta V_{SCO})_P$, corroborate the spin-state switching first witnessed by the color change of crystals, then by the magnetic and vibrational measurements. From the room temperature Raman spectra in Fig. 3b, it appears that the SCO process mainly takes place between 8.2 and 9.2 kbar. Although the quality of the data prevents the analysis of the cooperativity, we can observe a rather abrupt process going virtually to completion in ca. 1-2 kbar. This is more abrupt than the one observed by one of the authors in case of a cooperative and bistable 2D coordination network of $Fe(pyridine)_2[Ni(CN)_4]$ (at P = 1 bar, $T_{1/2}$ = 201 K, ΔT = 16 K; at T_{amb}, $P_{1/2}$ = 11 kbar, SCO spreading over *ca.* 8 kbar).[15,36]

From the magnetic measurements, a nearly linear correlation of the transition temperature $T_{1/2}$ with the applied pressure is apparent, which follows the expectation from the Clausius-Clapeyron relation. The fitted slope (ca. 16.4 (1.0) $Kkbar^{-1}$, Fig. 2b) is very close to those reported in the literature for different Fe(II) and Fe(III) SCO compounds (ranging typically between 10 - 20 $Kkbar^{-1}$).[7,9] The expression relating the pressure dependence of the transition temperature to the change of volume, that is $\partial T_{1/2}/\partial P = [(\Delta V_{HL})P/\Delta S_{HL}]$ may be quantitatively interpreted. If one takes into account the entropy change associated with the SCO[27] (ΔS_{HL} = 36.7 $Jmol^{-1}K^{-1}$ at atmospheric pressure) and the related volume change $((\Delta V_{HL})_P$ = 9.9 $Å^3$) one obtains a Clapeyron slope $(\partial T_{1/2}/\partial P$ = 16.2 K $kbar^{-1}$) and a transition pressure at ambient temperature ($P_{1/2}$ = 8.0 kbar), which are in remarkable agreement with the experimental results. It is worth noting that the validity of the Clausius-Clapeyron relationship was verified with data determined in presence of matrices of different nature. We can thus infer that in the 1-12 kbar pressure range, the observations are dominated by the intrinsic SCO features of $[Fe^{III}(3\text{-}OMeSalEen)_2]PF_6$. Since this compound is known to be sensitive to mechanochemical treatment, it can be inferred that the self-consistent description of the pressure effect observed with combined measurements derives from the crystalline nature of the sample and a quite good preservation of the pressure hydrostaticity.

3.4 Influence of the pressure-transmitting medium on the spin crossover

As described above, the embedding of the compound in the oils used as a pressure-transmitting medium systematically modifies the characteristics of the SCO curve at atmospheric pressure. Some of the authors have shown that the matrix characteristics (glassy, semi-crystalline state or melting) and the experimental conditions can be varied to tune efficiently the spin-crossover features (temperature shift, conversion smoothening and/or hysteresis opening). This 'matrix effect' was ascribed to elastic interactions established between molecules forming the matrix and the surface of the SCO microcrystals.[26,37,38] Besides the possible observation of progressive SCO, the opening of thermal hysteresis was accounted for by the cut off / switch on of these interactions activated by successive thermal glass- and spin-transitions of the matrix-crystals composite.[26] These experimental features were simulated by a mean-field approach based on negative variable external pressures together with a cut off/switch on of matrix-particles interactions.[37]

In the present work, the matrix effect also manifests as a downshift, smoothening and widening of the hysteresis loop in a fairly similar way for each medium used (Figure 1). The thermomechanical characteristics of the trade products used as matrices are not particularly well known, but their solidifications are expected to occur by lowering the temperature. To address this issue related to hydrostaticity in pressure cells, we performed DSC measurements of the different oils (see Figure S10 and comments in SI). The solidification occurs between 251 and 190 K (Alcatel 100), 197 and 168 K (Daphne 7373) or at T_g = 212 K (Fluorinert FC77), i.e. above (or close to) the SCO temperature (here at $T_{1/2}$ = 163 K). So the spin-transition curves observed in Figure 1 correspond to composites in the solid form. According to the studies of hydrostaticity in pressure transmitting media,[39-41] the solidification/vitrification of oils results in less homogenous environment (loss of hydrostaticity), a pressure deficit (negative pressure) and as a counterpart, possible deformations due to shear stress.[39] From that, we can expect a distribution of transition characteristics, in particular for the nucleation process, leading to more gradual curves and altered transition temperatures as observed. So given the sensitivity of SCO materials, this specific mechanical stress represents a plausible component of the matrix-particle interactions even if its magnitude and reversible character are hardly predictable.

Moreover, in the case of glassy Fluorinert FC77, we also notice changes in the spin transition features, which result from the composite ageing at 10 K. Such thermal history-dependent interactions and kinetic effect were previously pointed with glycerol glasses.[26,37] Interestingly, the hysteresis (see Fig. 1), shows the relatively narrow spreading of the descending and ascending branches (over ca. 15 K), which suggests limited matrix-crystal interactions in contrast with the case of glycerol or eicosan. The fact that the compressibility performances of perfluorocarbon oils derive from their weak cohesive intermolecular forces might be relevant.

With respect to the anomalies (steps) observed in our magnetic study performed under pressure (Figure 2), it should be noted that the limit of hydrostaticity of an oil as well as the spin transition characteristics vary according to a temperature-pressure phase diagram. As noted above, it seems unlikely that the temperature ranges of the Alcatel 100 solidification and the spin transition will overlap in our measurement conditions. In the absence of strong impact on the quality of the Clausius-Clapeyron correlation, the deviation of hydrostaticity

associated to the use of Alcatel 100 can be considered minor. The data reported in case of Fluorinert FC77 show a limit of hydrostaticity close to 9-10 kbar at ambient temperature[33] and thus, similar slight deviation related to solidification can occur just above the transition pressure of the compound under study.

Finally, it may be worth to note also that from recent investigations of SCO nanoobjects, it was inferred that the volume-dependent elastic cooperativity weakens at the nanoscale, so that the surface-related phenomena prevail.[3] Matrices in which the particles are embedded or the shells surrounding the particles are known to considerably influence the SCO characteristics.[26,42] As a consequence, the interface, matrix and thus confinement effects have to be further investigated.

Conclusions

We report the pressure-dependent properties of a well-known first-order spin-transition compound formed with a Fe(III) Schiff base, the cooperative spin state switching of which is coupled to a relatively small change of molecular volume of 10.5 Å^3 at ambient pressure. By applying a quasi hydrostatic pressure to crystals of this compound, it is possible to observe magnetic behavior characterized by smoother SCO curves, which are shifted to high temperatures. On the other hand, the evolution of the Raman spectra is indicative of an abrupt, reversible and complete pressure-induced spin-state switching process. As shown by the Raman spectrometry and the X-ray diffraction data, the room temperature HS to LS switching requires a pressure of 8-9 kbar. This result is fully consistent with the extrapolation of the magnetic dataset (acquired in rather different experimental conditions) and also with thermodynamical considerations (Clausius-Clapeyron law). When considering the peculiar sensitivity of the compound to mechanochemical treatments, the present result appears rather unexpected. The X-ray crystallographic study of the unit-cell parameters confirms the satisfying reversibility of the process that is limited by a minor loss of crystallinity as observed after decompression from 15 kbar. The change of the unit-cell volume (ΔV_{HL} = 9.9 Å^3 per-unit formula) is slightly lower than the value determined upon varying the temperature. The trends shown by all the parameters correspond to those of the thermal process if one discards the variations of the *a* and *c* axes which are presumably dominated by the high compressibility of the triclinic lattice. One additional aspect highlighted in this work relies on the effect of the matrix used in order to provide hydrostatic conditions on the spin transition behavior. This effect has been observed at the micrometric scale with single crystals. We plan to investigate in a future work this matrix effect on the thermally-induced spin transition properties of [Fe^{III}(3-OMeSalEen)$_2$]PF$_6$ when prepared in the form of micro- and nanocrystals. The dispersion in matrices of different nature would help to elucidate matrix-particle interactions at the origin of these new behaviors.

Experimental

Materials

Polycrystalline powder and dark brown single crystals of [Fe(3-OMeSalEen)$_2$]PF$_6$ have been obtained following the procedure described in Ref. 23b and 24, respectively. Elemental analysis (%) Calcd (Found) for C$_{26}$H$_{40}$F$_6$FeN$_4$O$_4$P: C, 44.80 (44.95); H, 5.33 (5.45); N, 8.71 (8.81).

Different oils were selected as pressure-transmitting medium in crystallographic, magnetic and Raman spectroscopic investigations on the basis of their hydrostaticity and other specific criteria (viscosity, optical properties, etc). These oils are Alcatel 100 (a paraffin-based mineral oil from Alcatel), Fluorinert FC77‡ (a perfluorocarbon liquid from 3M) and Daphne 7373 (a mixture of olefin oligomers from Idemitsu Kosan Global).

X-ray crystallography measurements.

A single-crystal of the compound and a few small ruby spheres were mounted in a Merrill-Bassett diamond anvil cell equipped with Boehler-Almax diamonds with culets of 600 µm. A 250 µm thick stainless steel gasket with a 350 µm diameter hole was used to form the sample chamber. Fluorinert FC-77 (3M^{TM} company) was used as a pressure-transmitting medium to ensure a hydrostatic pressure environment for the sample. Pressure was determined using the ruby fluorescence method.[43] High pressure X-ray diffraction data were collected on an Agilent Gemini diffractometer using graphite-monochromated Mo-Kα radiation (λ =0.71073 Å) radiation. Determination and refinement of cell parameters was performed using CrysAlisPro.[44] Due to the constraints of the DAC and low symmetry of the system, data completeness to 0.8 Å was less than 35%, and reliable refinement of structural detail was not possible.

Magnetic measurements.

Magnetic susceptibility measurements were performed using a Quantum Design SQUID magnetometer (MPMS5S Model) calibrated against a standard palladium sample. A batch of as-synthesized small crystals was studied between 250 and 120 K with a 0.5 Kmin^{-1} scanning rate. The same batch was used for studying the magnetic behavior of the crystals once dispersed in each of the oils selected for the pressure-dependent measurements. All the data in Figure 1 were collected between 180 and 140 K at a scanning rate of 0.5 Kmin^{-1} with an iterative regression algorithm. The measurements under pressure were carried out using a non-magnetic clamp cell with ~10 mg of single crystals of [Fe(3-OMeSalEen)$_2$]PF$_6$ dispersed in ~20 mg Alcatel 100 oil. The superconducting transition temperature of Pb (≈ 7 K), depending linearly on the pressure, was used to calibrate the pressure and verify the hydrostatic conditions (Fig. S7 in SI). The temperature was varied with a speed of 0.5 Kmin^{-1} while the pressure was clamped at fixed values between 0 and 6.5 kbar. Each curve was measured twice. The raw magnetization data are reported because no reliable χ$_M$ values could be extracted for the large uncertainty on the sample mass and the diamagnetic contribution. Further details on the high pressure magnetic

measurement setup and protocol have been published in ref. 25

Raman spectrometry measurements

Raman spectra were acquired using a microspectrometer (Xplora, Horiba) equipped with a λ_{exc} = 638 nm laser. The laser beam was focused on the sample with a long-working-distance objective (50×, numerical aperture = 0.5), which was also used to collect the scattered photons. The laser intensity (ca. 0.1 mW) was carefully adjusted to avoid unwanted laser-induced heating. During the experiments the orientation of the sample crystal was kept constant with respect to the polarization direction of the laser. Using a 1800 grooves/mm grating a spectral resolution of ca. 4 cm^{-1} was achieved. The pressure cell and the associated sample loading protocol were the same as described for XRD measurements except that simple (Drukker cut) diamonds were used and the pressure transmitting medium was Daphne 7373 oil. Fig. S8 in the SI shows the luminescence spectra of ruby that enabled the calibration of the pressure.

Differential Scanning Calorimetry measurements.

DSC measurements were carried out on a Netsch DSC 204 Instrument under Helium purging gas (30 cm^{3}min^{-1}) at a heating/cooling rate of 10 Kmin^{-1}. The temperature and enthalpy values were calibrated using the melting transition of standard materials (Hg, In, Sn).

Conflicts of interest

There are no conflicts to declare.

Acknowledgements

Notes and references

‡ Footnotes:
- See the chemical and physico-chemical properties provided by the supplier, http://extcon.co.uk/fc74/info.pdf.

1   Spin Crossover in Transition Metal Compounds I−III, in *Top. Curr. Chem.*, ed. P. Gütlich and H. A. Goodwin, Springer, Berlin, 2004, vol.233-235.
2   *Spin Crossover Materials: Properties and Application*, ed. M.A. Halcrow, Wiley, Chichester, UK, 2013.
3   G. Molnár, S. Rat, L. Salmon, W. Nicolazzi and A. Bousseksou, *Adv. Mat.*, 2018, **30**, 17003862.
4   P. Guionneau, M. Marchivie, G. Bravic, J.-F. Létard and D. Chasseau, *Top. Curr. Chem.*, 2004, **234**, 97.
5   V. Ksenofontov, A.B. Gaspar and P. Gütlich, *Top. Curr. Chem.*, 2004, **235**, 23.
6   J. A. Real, A. B. Gaspar and M. C. Munoz, *Dalton Trans.*, 2005, 2062-2079.
7   G. G. Levchenko, A. V. Khristov and V. N. Varyukhin, *Low Temp. Phys.*, 2014, **40**, 571-585.
8   J. P. Tidey, H. L. S. Wong, M. Schröder and A. J. Blake, *Coord. Chem. Rev.*, 2014, **277-278**, 187-207.
9   (a) P. Gütlich, V. Ksenofontov and A. B. Gaspar, *Coord. Chem. Rev.*, 2005, **249**, 1811-1829; (b) P. Gütlich, A. B. Gaspar, Y. Garcia and V. Ksenofontov, *C. R. Chim.*, 2007, **10**, 21-36.
10 H. J. Shepherd, T. Palamarciuc, P. Rosa, P. Guionneau, G. Molnár, J.-F. Létard and A. Bousseksou, *Angew. Chem. Inter. Ed.*, 2012, **51**, 3910-3914.
11 H. Spiering, *Spin Crossover in Transition Metal Compounds III*, Springer Berlin Heidelberg, Berlin, Heidelberg, 2004, pp. 171-195.
12 P. Gütlich, A. Hauser and H. Spiering, *Angew. Chem. Int. Ed.*, 1994, **33**, 2024-2054.
13 (a) M. Nishino, K. Boukheddaden, Y. Konishi and S. Miyashita, *Phys. Rev. Lett.*, 2007, **98**, 247203 (b) C. Enachescu, L. Stoleriu, A. Stancu and A. Hauser, *Phys. Rev. Lett.*, 2009, **102**, 257204; (c) C. Enachescu and A. Hauser, *Phys. Chem. Chem. Phys.*, 2016, **18**, 20591-20599; (d) W. Nicolazzi, S. Pillet and C. Lecomte, *Phys. Rev. B*, 2008, **78**, 174401.
14 M.-L. Boillot, J. Zarembowitch, J.-P. Itié, A. Polian, E. Bourdet and J. G. Haasnoot, *New J. Chem.*, 2002, **26**, 313-322.
15 G. Molnár, T. Kitazava, L. Dubrovinsky, J. J. McGarvey and A. Bousseksou, *J. Phys.: Cond. Matt.*, 2004, **16**, S1129.
16 V. Ksenofontov, A. B. Gaspar, G. Levchenko, B. Fitzsimmons and P. Gütlich, *J. Phys. Chem B*, 2004, **108**, 7723-7727.
17 G. Levchenko, A. Khristov, V. Kuznetsova and V. Shelest, *J. Phys. Chem Sol.*, 2014, **75**, 966-971.
18 A. H. Ewald, R. L. Martin, E. Sinn and A. H. White, *Inorg. Chem.*, 1969, **8**, 1837-1846.
19 A. Tissot, H. J. Shepherd, L. Toupet, E. Collet, J. Sainton, G. Molnár, P. Guionneau and M.-L. Boillot, *Eur. J. Inorg. Chem.*, 2013, **2013**, 1001-1008.
20 P. Á. Szilágyi, S. Dorbes, G. Molnár, J. A. Real, Z. Homonnay, C. Faulmann and A. Bousseksou, *J. Phys. Chem Sol.*, 2008, **69**, 2681-2686.
21 R. Bertoni, M. Lorenc, H. Cailleau, A. Tissot, J. Laisney, M.-L. Boillot, L. Stoleriu, A. Stancu, C. Enachescu and E. Collet, *Nat. Mat.*, 2016, **15**, 606.
22 A. Tissot, L. Rechignat, A. Bousseksou and M.-L. Boillot, *J. Mater. Chem.*, 2012, **22**, 3411-3419.
23 (a) M. S. Haddad, W. D. Federer, M. W. Lynch and D. N. Hendrickson, *J. Am. Chem. Soc.*, 1980, **102**, 1468-1470; (b) M. S. Haddad, M. W. Lynch, W. D. Federer and D. N. Hendrickson, *Inorg. Chem.*, 1981, **20**, 123-131; (c) M. S. Haddad, W. D. Federer, M. W. Lynch and D. N. Hendrickson, *Inorg. Chem.*, 1981, **20**, 131-139..
24 A. Tissot, R. Bertoni, E. Collet, L. Toupet and M.-L. Boillot, *J. Mater. Chem.*, 2011, **21**, 18347-18353.
25 G. Molnár, T. Guillon, N. Ould-Moussa, L. Rechignat, T. Kitazawa, M. Nardone and A. Bousseksou, *Chem. Phys. Lett.*, 2006, **423**, 152–156.
26 A. Tissot, C. Enachescu and M. L. Boillot, *J. Mater. Chem.*, 2012, **22**, 20451-20457.
27 M. Sorai, R. Burriel, E. F. Westrum and D. N. Hendrickson, *J. Phys. Chem. B*, 2008, **112**, 4344-4350.
28 M. J. Cliffe and A. L. Goodwin, *J. Appl. Cryst.* 2012, **45**, 1321; http://pascal.chem.ox.ac.uk/
29 J. Jung Ph-D Thesis, D77, Johannes Gutenberg-Universität Mainz (1995)
30 T. Granier, B. Gallois, J. Gaultier, J. A. Real and J. Zarembowitch, *Inorg. Chem.*, 1993, **32**, 5305-5312.
31 M. Mikolasek, M. D. Manrique-Juarez, H. J. Shepherd, K. Ridier, S. Rat, V. Shalabaeva, A.-C. Bas, I. Collings, A. Chumakov, T. Leichle, L. Nicu, W. Nicolazzi, G. Molnár, L. Salmon, A. Bousseksou, to be submitted.

32 H. J. Shepherd, P. Rosa, L. Vendier, N. Casati, J.-F. Létard, A. Bousseksou, P. Guionneau and G. Molnár *Phys. Chem. Chem. Phys*., 2012, **14**, 5265–5271

33 G. Félix, M. Mikolasek, H. J. Shepherd, J. Long, J. Larianova, Y. Guari, J.-P. Itié, A. I. Chumakov, W. Nicolazzi, G. Molnár and A. Bousseksou *Eur. J. Inorg. Chem*. 2018, 443-448.

34 A. Bleuzen, J.-D. Cafun, A. Bachschmidt, M. Verdaguer, P. Münsch, F. Baudelet and J.-P. Itié *J. Phys. Chem. C* 2008, **112**, 17709.

35 K. Boukheddaden, E. D. Loutete-Dangui, E. Codjovi, M. Castro, J.A. Rodriguéz-Velamazán, S. Ohkoshi, H. Tokoro, M. Koubaa, Y. Abid and F. Varret *J. Appl. Phys.* 2011, **109**, 013520.

36 K. Hosoya, T. Kitazawa, M. Takahashi, M. Takeda, J.-F. Meunier, G. Molnar and A. Bousseksou, *Phys. Chem. Chem. Phys.*, 2003, **5**, 1682-1688.

37 R. Tanasa, J. Laisney, A. Stancu, M.-L. Boillot and C. Enachescu, *Appl. Phys. Lett.*, 2014, **104**, 031909.

38 C. Enachescu, R. Tanasa, A. Stancu, A. Tissot, J. Laisney and M.-L. Boillot, *Appl. Phys. Lett.*, 2016, **109**, 031908.

39 K. Yokogawa, K. Murata, H. Yoshino and S. Aoyama, *Jpn. J. Appl. Phys*., 2007, **46**, 3636-3639.

40 (a) T. Varga, A. P. Wilkinson and R. J. Angel, *Rev. Sci. Instrum.*, 2003, **74** 4564; (b) V A Sidorov and R A Sadykov, *J. Phys.: Condens. Matter,* 2005, **17**, S3005–S3008.

41 M. S. Torikachvili, S. K. Kim, E. Colombier, S. L. Bud'ko, and P. C. Canfield *Rev. Sci. Instrum.*, 2015, **86**, 123904,1-18.

42 Y. Raza, F. Volatron, S. Moldovan, O. Ersen, V. Huc, C. Martini, F. Brisset, A. Gloter, O. Stephan, A. Bousseksou, L. Catala and T. Mallah, *Chem. Comm.*, 2011, **47**, 11501-11503.

43 G. J. Piermarini, S. Block, J. D. Barnett and R. A. Forman, *J. Appl. Phys.*, 1975, **46**, 2774-2780.

44 CrysAlis Pro, A. Oxford Diffraction Ltd, Version 1.171.37.33 edn.